# Atomic modeling for the initial stage of chromium passivation

*Li-nan Zhang*[1,2,3], *Xi-lin Xiong*[1,2], *Yu Yan*[1,2], *Ke-wei Gao*[1,2], *Li-jie Qiao*[1,2], *and Yan-jing Su*[1,2]

1) Beijing Advanced Innovation Center for Materials Genome Engineering, University of Science and Technology Beijing, Beijing 100083, China

2) Corrosion and Protection Center, Key Laboratory for Environmental Fracture (MOE), University of Science and Technology Beijing, Beijing 100083, China

3) SUNCAT Center for Interface Science and Catalysis, SLAC National Accelerator Laboratory, Menlo Park, CA 94025, USA

**Abstract:** The well-known anti-corrosive property of stainless steels is largely attributed to the addition of Cr, which can assist in forming an inert film on the corroding surface. To maximize the corrosion-resistant ability of Cr, a thorough study dealing with the passivation behaviors of this metal, including the structure and composition of the passive film as well as related reaction mechanisms, is required. Here, continuous electrochemical adsorptions of OH-groups of water molecules onto Cr terraces in acid solutions are investigated using DFT methods. Different models with various surface conditions are applied. Passivation is found to begin in the active region, and a fully coated surface mainly with oxide is likely to be the starting point of the passive region. The calculated limiting potentials are in reasonable agreement with passivation potentials observed via experiment.
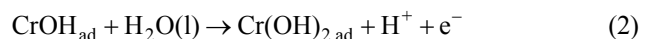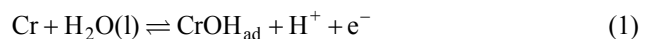
**Keywords:** chromium; acid solutions; passive films; interfaces; modeling studies

## 1. Introduction

Corrosion, occurring throughout the world, is largely responsible for the huge amounts of metal losses in the steel industry annually [1], with nearly half of the iron production used to replace the deteriorated structures caused by corrosion [2]. Hence, there is a great demand for finding ways to reduce or even eliminate the occurrence of corrosion. Currently, using alloying elements (Cr, Ni, Cu, Ti, etc.) for the control of corrosion of steels is a widely accepted practice [3–8].

Among the numerous anti-corrosive alloying agents, chromium has been demonstrated to be one of the most beneficial constituents in stainless steels (notable for the corrosion resistance). To date, huge bulks of works have been devoted to the investigation of stainless steels or Fe–Cr alloys [9–19]. Cr is found to have an effect in the formation of an inert film on the surface that has very flexible structure and constantly changes in thickness and composition to accommodate the corrosive environment. Despite those remarkable works, several aspects relating to the passivation behaviors of pure Cr still remain controversial and require further understanding.

The adsorption theory of passivity states that the chemical reactivity of metals can be diminished as long as the metal surface or even only the most reactive facet is covered with oxygen (or oxygen containing groups) [20–21]. The passivation of Cr may proceed via a direct reaction with water (working as oxygen reservoir) [22–24]. Okuyama *et al.* [25] propose that, in dilute acid solutions, the passivation process involves a hydroxyl intermediate and occurs in parallel with the active anodic dissolution. Alternatively, Björnkvist and Olefjord [26] suggest that the first oxidation step is a reversible formation of Cr(I)-hydroxide; the second step, the formation of adsorbed Cr(OH)$_2$, is taken as the rate determining step, followed by either oxidation to trivalent oxy-hydroxide or chemical dissolution to the chromous ion. This mechanism is proposed as follows:

$$Cr + H_2O(l) \rightleftharpoons CrOH_{ad} + H^+ + e^- \qquad (1)$$

$$CrOH_{ad} + H_2O(l) \rightarrow Cr(OH)_{2,ad} + H^+ + e^- \qquad (2)$$

$$Passivation: \ Cr(OH)_{2,ad} \rightleftharpoons CrOOH_{ad} + H^+ + e^- \qquad (3)$$

$$Dissolution: \ Cr(OH)_{2,ad} + 2H^+ \rightleftharpoons Cr^{2+} + 2H_2O(l) \qquad (4)$$

Characterization of the atomic structure and chemical composition of the passive film is very difficult to perform.

🐾 Springer

Uhlig [20–21] considers the passive layer on transition metals as thin non-stoichiometric chemisorbed oxide of variable hydrogen content, which is sometimes less than a monolayer in thickness. Different measurement techniques indicate that the passive film on Cr is composed only of hydrated trivalent chromic species [9,14,27–31]. Moffat and Latanision [28] describe the film as amorphous hydrated chromic oxide — chromic ions bridged by water, hydroxide, and/or oxide ligands, leading to a significant degree of bonding flexibility, which is vital for its high protective quality. Stypula and Banaś [29] indicate that, irrespective of acid concentration, the average composition of the film is nearly equal to Cr(III) oxy-hydroxides. Maurice *et al.* [30] and Zuili *et al.* [31] suggest a bilayer structure for the passive film, which may consist of a hydroxide layer in the outer part and oxide layers in the inner part along with some amount of oxy-hydroxide.

Nowadays, researchers use atomistic modeling techniques to establish links between electronic structure calculations and macroscopic corrosion properties. Ma *et al.* [32] have developed a model to evaluate the active dissolution behavior of metals/alloys using outputs obtained from DFT methods. For blunt metals, the interest in passivity is focused on the chemical stability of the passive films, or rather, the electronic energy levels of various surface states during passivation [33]. As the characteristics of the passive film are confirmed as a function of potential and time [17,28,30–31,34–35], the potential is probably a useful parameter that describes dynamically the anodic behavior of the metal surface losing electrons in the presence of corrosive medium and monitors the rate of electrochemical reactions blocking corrosion.

In this work, first principle calculations have been performed to investigate the passivation properties for pure Cr in acid solutions. The mechanism is illustrated by stepwise electrochemical adsorption of hydroxyl, dissociated from water, onto Cr terraces. We predict how the passive monolayer forms and how it contributes to the electrode potential at the initial stage of passivation. The calculated intrinsic limiting potential is in reasonable agreement with experimentally obtained passivation potential. Different pH conditions have been tested.

## 2. Computational methods

### 2.1. Density functional theory

During corrosion, surface is always the first part to get in touch with the corrosive environment. Surfaces with different orientations have different corrosion behaviors [36–39].

Generally, the dominant structure available for charge transfer is the terrace [40–43]. Here, we limit our study to the most stable close-packed surface, Cr(110), using the optimized lattice constant of 0.2866 nm. The surface is modeled by a periodically repeated 3×3 four-layer slab, separated by at least 1.5 nm of vacuum in the z-direction of the interface. The two bottom layers are fixed, and the other layers and the adsorbates are geometrically relaxed so that the maximum force in any direction on any moveable atom is less than 0.5 eV/nm. Dipole corrections are included in all cases to decouple the electrostatic interaction between periodically repeated slabs.

The most stable chemisorption site for both *OH and *O (* denotes an available surface site) species is the 3-fold hollow site on Cr(110). Several possible adsorption configurations have been tested in each case. By calculating the vibrational frequencies for all the intermediates, zero-point energy (ZPE) corrections are included and the entropy and enthalpy under specific reaction conditions can be determined.

In addition, water can clearly stabilize the *OH species due to formation of H-bond but not to *O [44–45]. Therefore, the solvation effect is explicitly taken into account in this work by comparing the free energy difference between OH adsorbed on the chromium surface with and without the water environment (a hexagonal bilayer network [46–47]). The electric field effect on the adsorption energies appears to be negligible [48]. Thus, the change in free energy is given by:

$$\Delta G^{\ominus} = \Delta E + \Delta E_{w,water} + \Delta ZPE - T\Delta S \tag{5}$$

where $\Delta E$ is the reaction energy of each intermediate step, $\Delta ZPE$ is the zero-point energy correction, $\Delta S$ is the entropy change, $T$ is temperature, and $\Delta E_{w,water}$ with the value of $-0.17$ eV is used as an estimation for the water induced stabilization energy per *OH species. The solvation effect has not been applied to the *O species.
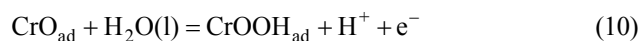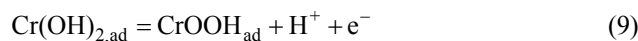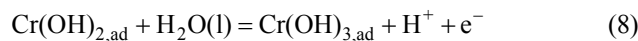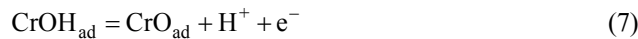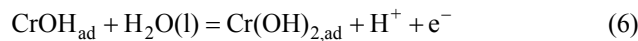
Our electronic calculations are carried out using Quantum Espresso software package [49], interfaced with the atomic simulation environment (ASE) [50]. Ionic-core interactions are represented via relativistic Vanderbilt ultrasoft pseudopotentials [51]. Plane wave basis sets with kinetic energies up to 600 eV are used. The RPBE (revised Perdew-Burke-Ernzerhof) exchange correlation functional is selected for the more accurate estimation of chemisorption energies of small molecules on metal surfaces [52]. A Fermi-Dirac distribution with a smearing of 0.1 eV is applied. The k-points are sampled using a 4×4×1 Monkhorst-Pack grid [53]. Test calculations indicated that a denser k-points sampling made no significant changes in the configurations

and the adsorption energies (less than 0.01 eV). All the calculations are performed without spin-polarization.

## 2.2. Electrochemical treatment

On the basis of experimental findings, passivation of Cr is likely to occur without relation to active dissolution. At one area, diffusion controlled dissolution takes place, whereas, at another area, blocking of the surface by passivation is found to occur [17,36]. Hence, we focus only on the passivation process and follow the stepwise mechanism proposed by Björnkvist and Olefjord [26] (see Eqs. (1)–(3)). Similar mechanisms have been successfully applied in recent theoretical studies on aqueous Zn [54]/Al [40]/Mg [41]-air batteries.

However, after the first *OH adsorbed on the surface, the pathway can actually bifurcate. The following dissociated hydroxyl from the aqueous solution can either bind onto an available surface site or collide with a previously adsorbed *OH to reform water molecules. In other words, without regard to dissolution, the formation of each hydroxide is followed by either a continuous adsorption step to form higher-valence hydroxide or a deprotonation step to form oxide (or oxy-hydroxide), depending mainly on the thermostability of the corresponding product. To clarify the process, we test all the possible pathways followed by Eq. (1) as follows:

$$CrOH_{ad} + H_2O(l) = Cr(OH)_{2,ad} + H^+ + e^- \tag{6}$$

$$CrOH_{ad} = CrO_{ad} + H^+ + e^- \tag{7}$$

$$Cr(OH)_{2,ad} + H_2O(l) = Cr(OH)_{3,ad} + H^+ + e^- \tag{8}$$

$$Cr(OH)_{2,ad} = CrOOH_{ad} + H^+ + e^- \tag{9}$$

$$CrO_{ad} + H_2O(l) = CrOOH_{ad} + H^+ + e^- \tag{10}$$

In our calculations, all species are in their standard state, which defines a concentration of 1 M for aqueous species. As one of the aqueous species is $H^+$, this automatically implies that all chemical potentials within the reaction cycle are given at pH = 0. The chemical potential ($\mu$) of a proton-electron pair can be related to that of one-half hydrogen gas using the computational hydrogen electrode (CHE) [44]:

$$\mu_{H^+} + \mu_{e^-} = \frac{1}{2}\mu_{H_2(g)} \tag{11}$$

The effect of a bias on the free energy levels involving charge transfer is included by $-neU$:

$$\Delta G = \Delta G^{\ominus} - neU \tag{12}$$

where $U$ is the electrode potential, $e = 1.6 \times 10^{-19}$ C, and $n$ is the number of electrons transferred. All potentials given hereafter are referenced to the standard hydrogen electrode (SHE).

## 3. Results and discussions

### 3.1. Pourbaix diagram

To investigate the composition of the passive layer, the first step is to consider the electrochemical stability for different oxidation states of Cr. The energy associated with an element changing oxidation state is often described in terms of reduction potentials of the products involved. A Pourbaix diagram, shown in Fig. 1, exactly maps out possible bulk phase reactions of an element in an aqueous electrochemical system as a function of pH and potential (versus SHE) [55]. The Nernst equation is used to account for the pH effect on the standard electrode potentials for the reactions taking place during Cr oxidation. The reference potential $U_0$ is obtained from free bulk formation energies at pH = 14 [56].
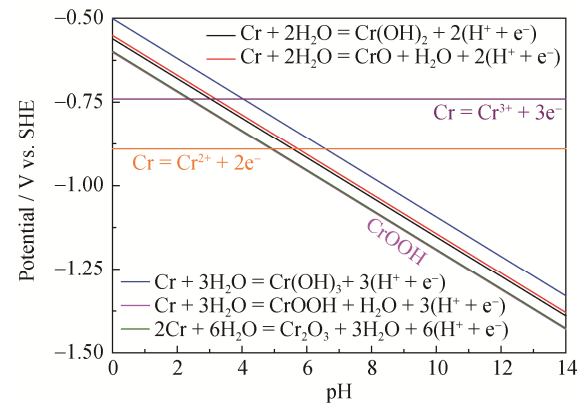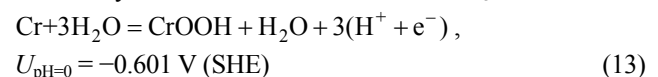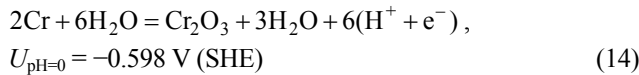
**Fig. 1. Pourbaix diagram mapping out the possible bulk reactions during chromium oxidation. All the reactions start with bulk chromium and liquid water, with the exception of $Cr^{2+}$ and $Cr^{3+}$, within which chromium dissolves to ions directly.**

The formation of oxy-hydroxide (CrOOH) from bulk Cr is most chemically favorable. The chemical stability of the oxide ($Cr_2O_3$) is quite comparable to that of the oxy-hydroxide, whereas the formation of bulky hydroxide ($Cr(OH)_3$) is rather unfavored. The products of the second oxidation step, namely, $Cr(OH)_2$ and CrO, are quite similar in stability. The dissolution product in acid solutions is chromous ions ($Cr^{2+}$), which is in line with experimental results [17,25–26].

From Fig. 1, we can also determine the reduction potentials for each bulk reaction at a target pH. At pH = 0, without regard to dissolution, solid Cr reacts with water to form chemically more stable bulk CrOOH or $Cr_2O_3$ at the anode:

$$Cr + 3H_2O = CrOOH + H_2O + 3(H^+ + e^-),$$
$$U_{pH=0} = -0.601 \text{ V (SHE)} \tag{13}$$

$$2Cr + 6H_2O = Cr_2O_3 + 3H_2O + 6(H^+ + e^-),$$
$$U_{pH=0} = -0.598 \text{ V (SHE)} \qquad (14)$$

Here, the review of the thermodynamic data gives only a rough insight into the passive layer. The potentials given here are determined from the free energy changes between bulk phases. The anode potential must be higher than those values because the crystallization of bulky items are accompanied by a large chemical stabilization, which cannot contribute to electrode potentials [40]. Evidence from other studies indicate that the variation in oxidation states of Cr occurs mainly in the first layers of the film near the interfaces [19,35]. Thus, next, we move on to simulate the stepwise passivation mechanism of Cr in acid solutions to gain more insight into the elementary steps (see Eqs. (1), (6)–(10)) occurred on the interface, which truly count in the formation of the passive film as well as the corresponding electrode potentials.

### 3.2. Free energy diagrams (FED)

As elucidated in the method part and based on Eqs. (1), (6)–(10), we construct the Gibbs free energy diagram for all possible intermediate reactions involved in the passivation process occurred on Cr(110) in acid solutions (pH = 0). The results on a bare terrace are shown in Fig. 2.
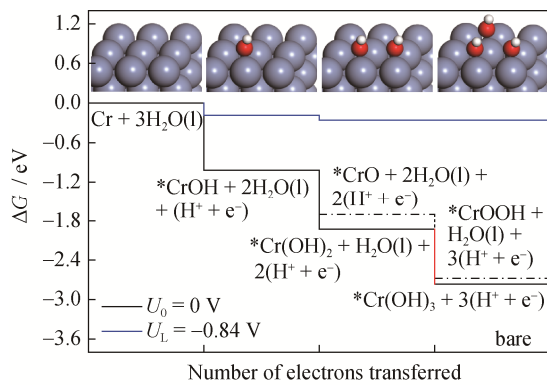


**Fig. 2. Free energy diagram for the stepwise Cr passivation on a bare (110) close-packed surface at pH = 0. Black line: all calculations are done at $U_0 = 0$ V (SHE). The most possible reaction states are shown in bold and the configurations of the corresponding intermediate species are illustrated in the insets. Blue line: the limiting potential ($U_L$) required to run all the elementary steps exothermically. The limiting step is shown in red.**

At $U = 0$ V (SHE), the value of $\Delta G$ between individual surface states corresponds to the difference in the adsorption energies of relevant intermediate species. As shown in Eq. (12), the $\Delta G$ of an elementary step involving charge transfer

is a function of potential. As the potential is shifted more negative (positive) versus SHE, $\Delta G$ is raised (decreased) according to $\Delta G = -neU$. Thus, there exists a limiting potential ($U_L$) at which the reaction is downhill in free energy at each step, that is, a reasonable rate can be achieved [57]. The limiting potential is governed by the strength of adsorption, or, is determined by the composition and structure of the passive layer as well as related intermediate reactions; this dependence is similar to the characterization of passivation potentials (the most negative electrode potential at which the passive film forms.). At this point, we have bridged a link between the microscale electrochemical calculation and the macroscopic passivation property.

In Fig. 2, each elementary step on a bare Cr(110) terrace is downhill at $U_0 = 0$ V (SHE). Due to the solvation effect on *OH species but not on *O, the hydroxides bind much stronger to the surface than the oxides or oxy-hydroxide under same valence state of Cr, making them as the dominating products. Hence, the possible reaction path is Cr → *CrOH → *Cr(OH)$_2$ → *Cr(OH)$_3$. Then, there exists a lowest potential below which the free energy of at least one step is shifted uphill and will have a thermodynamic barrier. The potential determining step is the oxidation of Cr(II)-hydroxide giving Cr(III)-hydroxide, and the corresponding potential is −0.84 V (SHE).

According to the polarization curves recorded on Cr(110) in 0.5 M H$_2$SO$_4$ [30–31], such a negative value required indicates that the surface is currently in the active region, where anodic dissolution dominates. As adsorption steps are largely exergonic, with increasing applied potential, a rapidly dissociated chemisorption of water must occur before entering the passive region. Hence, the surface is expected to be highly covered, that is, the low coverage case cannot be used to calculate the passivation potential. So, in the following, a high coverage scheme is applied.

First, an *OH-covered surface with coverage of *N*-2 (*N* is the number of active surface adsorption site) is used, a coverage at which the surface can be fully covered after an oxidation cycle (see Eqs. (1)–(3)). Unfortunately, multiple *OH adsorptions on the terrace are quite unstable, even at relatively low coverages. The intense interaction between the *OH species allows the dehydration to easily occur, indicating that we can hardly have a densely *OH-covered terrace. Alternatively, the evidenced increase in the thickness of oxide in the passive layer [30–31] suggests that an *O-rich case may be more appropriate. The results of the case with *O-coverage of *N*-2 are shown in Fig. 3.
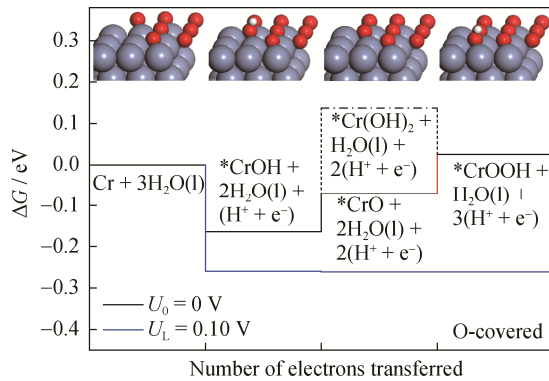
**Fig. 3.** **Free energy diagram for the stepwise Cr passivation on the (110) close-packed surface at pH = 0, starting with $*O_{N-2}$ ($N$ is the number of active surface adsorption sites). Black line: all calculations are done at $U_0 = 0$ V (SHE). The most possible reaction states are shown in bold and the configurations of the corresponding intermediate species are illustrated in the insets. Blue line: the limiting potential ($U_L$) required to run all the elementary steps exothermically. The limiting step is shown in red.**

On an $*O$-rich Cr(110) surface, the free energy plot differs much from that on a bare surface. The reaction is endothermic at $U_0 = 0$ V (SHE). For the second oxidation step, deprotonation to form $*CrO$ is preferred with a smaller thermodynamic driving force. For the third step, the formation of Cr(III)-hydroxide is prohibited under current coverage because it is followed by an immediate dehydration step. We have also considered a lower coverage case ($N$-3), showing that the $*Cr(OH)_3$ state is very thermodynamically unstable compared to $*CrOOH$ (0.67 eV higher in free energy). Hence, the probable passivation path is Cr → $*CrOH$ → $*CrO$ → $*CrOOH$.

The most endergonic step is the addition of the third $*OH$ to form $*CrOOH$, and a minimum potential of 0.10 V (SHE) is required for all the steps to be exergonic, which is positive and significantly higher than the value determined on a bare terrace (−0.84 V (SHE) in Fig. 2). This observation is easy to understand. The previously formed adsorbates can reduce the chemical reactivity of the metal surface and thereby inhibit further adsorptions; as a result, the process of anodic discharge becomes sluggish. However, at the cathode, a great amount of electrons are still largely consumed, resulting in the requirement of additional driving forces to promote anodic discharge. Therefore, the electrode potential is shifted in the positive direction.

The limiting potential determined here is quite comparable to the experimentally observed passivation potential of ~0 V (SHE) for Cr(110) in 0.5 M $H_2SO_4$ [30–31], substantiating the $*O$-rich scheme as a reasonable model for depicting the surface states at the beginning of the passive re-

gion. The model reveals that a monolayer thick passive film with a major component of oxides with some amount of oxy-hydroxides is formed before entering the passive region.

Further, the passivation potential obtained from the polarization plot for a Cr electrode passivated in borate buffer solution (pH = 8.4) [34] is ~0.36 V (SHE), while our value calculated using the $*O$-covered model at this pH is 0.59 V (SHE). As demonstrated by Dobbelaar and De Wit [36], the passivation potential for single crystal is more positive than that for polycrystalline Cr. Thus, our theoretical value is in high accordance with the experimental one, which helpfully verifies the reliability of our current model.

### 3.3. Formation of the passive monolayer

Based on the results above, we delineate the formation of the passive monolayer at the initial stage of Cr passivation in an acid solution in Fig. 4. The curve is roughly divided into four regions: 1) the active region where anodic dissolution dominates, 2) the active-passive transition region where passivation starts to compete with dissolution, 3) the passive region where passive film forms and thickens, and 4) the transpassive region where the thin film dissolves and corrosion rate increases again.
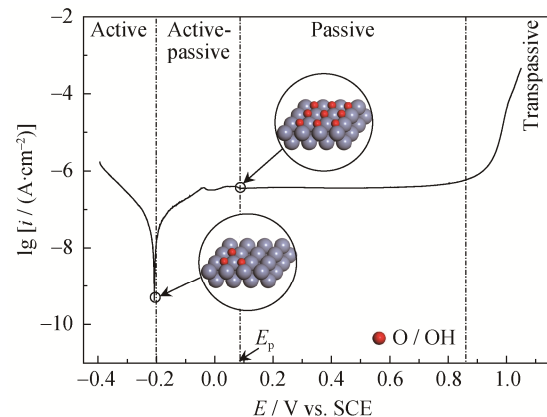


**Fig. 4.** **Anodic polarization curve recorded on a Cr electrode in 0.5 M $H_2SO_4$ at a scanning rate of 0.5 mV/s. The observed passivation potential ($E_p$) is highlighted. Two surface configurations with different adsorbate coverage are shown to illustrate the initial passive monolayer forming process occurring at the Cr-acid solution interface.**

As shown in Fig. 4, pure Cr corrodes when immersed in an acid solution at negative potentials, forming the active region. At slightly higher potentials, the formation of passive film begins in the active region via chemisorbed adsorption of water (illustrated by the low coverage case) and continues with increasing potential. This is in consistent

with the conclusion stated by Bojinov *et al.* [19] that the adsorption-driven passivation process starts shortly after the peak of active dissolution on the polarizing curve. The separately occurring passivation process competes with the anodic dissolution, forming the active-passive transition region.

As more oxidizing agent is added, the fully coating of the metallic Cr surface (illustrated by the high coverage case) is then considered as the beginning of the passive region. The passive monolayer formed here contains oxide mainly with some amount of oxy-hydroxide. The corresponding electrode potential is defined as the passivation potential ($E_p$). Upon increasing potentials and/or time of passivation, thickening and changing in the chemical composition of the passive layer occurs simultaneously [19]. The passive monolayer may constantly grow by crystallization of oxide deep into the inner part and multilayer adsorption of hydroxyl forming hydroxide outer part. Then the passive film can be viewed as an oxide inner layer (containing some oxy-hydroxide) having a hydroxylated shell surface [30–31]. At very positive potentials, this thin film will dissolve and the corrosion rate increases again, forming the transpassive region.

## 4. Conclusions

The high reaction rates and small dimensions of passive layer make the study of corrosion protection complicated and intractable. A combination of various experimental techniques must be applied to obtain a reliable picture of a specific system. Nevertheless, it can be scarcely possible to detect the surface states at the initial stage of the passivation process via experiment.

In this work, DFT methods have been applied to investigate the elementary steps involved in the initial stage of Cr passivation in acid solutions. The hydroxylation reaction of Cr proceeds with possible Cr(OH) and Cr(OH)$_2$ (or CrO) intermediate states.

According to the results, the passivation related adsorption of water occurs readily and continuously from the active region and competes with anodic dissolution. Then, a model with an *O-coverage of near unity is considered as appropriate for representing surface state at the beginning of the passive region. The calculated limiting potential, determined by the energy states of the surface layer as well as related intermediate reactions, is in reasonable agreement with experimentally measured passivation potential. The comparability with experimental data at a higher pH further confirms the reliability of our model.

By this contribution, we try to provide some new insights at the atomic scale into the computational modeling of surface reactions governing the passivation properties and the design of better anti-corrosion materials. The investigations of passivation potential for planes with orientations different from (110) and the passivation processes that occurred on other metal surfaces are topics of our future studies.

## Acknowledgement

## References

[1]    X.G. Li, D.W. Zhang, Z.Y. Liu, Z. Li, C.W. Du, and C.F. Dong, Materials science: share corrosion data, *Nature*, 527(2015), p. 441.

[2]    N. Ahmad and A.G. MacDiarmid, Inhibition of corrosion of steels with the exploitation of conducting polymers, *Synth. Met.*, 78(1996), No. 2, p. 103.

[3]    T. Misawa, K. Asami, K. Hashimoto, and S. Shimodaira, The mechanism of atmospheric rusting and the protective amorphous rust on low alloy steel, *Corros. Sci.*, 14(1974), No. 4, p. 279.

[4]    M. Stratmann, K. Bohnenkamp, and T. Ramchandran, The influence of copper upon the atmospheric corrosion of iron, *Corros. Sci.*, 27(1987), No. 9, p. 905.

[5]    T. Nishimura, H. Katayama, K. Noda, and T. Kodama, Effect of Co and Ni on the corrosion behavior of low alloy steels in wet/dry environments, *Corros. Sci.*, 42(2000), No. 9, p. 1611.

[6]    T. Ujiro, S. Satoh, R.W. Staehle, and W.H. Smyrl, Effect of alloying Cu on the corrosion resistance of stainless steels in chloride media, *Corros. Sci.*, 43(2001), No. 11, p. 2185.

[7]    Y.S. Choi, J.J. Shim, and J.G. Kim, Effects of Cr, Cu, Ni and Ca on the corrosion behavior of low carbon steel in synthetic tap water, *J. Alloys Compd.*, 391(2005), No. 1-2, p. 162.

[8]    A. Pardo, M.C. Merino, A.E. Coy, F. Viejo, M. Carboneras, and R. Arrabal, Influence of Ti, C and N concentration on the intergranular corrosion behaviour of AISI 316Ti and 321 stainless steels, *Acta Mater.*, 55(2007), No. 7, p. 2239.

[9]    N. Hara and K. Sugimoto, The study of the passivation films on Fe–Cr alloys by modulation spectroscopy, *J. Electrochem. Soc.*, 126(1979), No. 8, p. 1328.

[10]   M. Keddam, O.R. Mattos, and H. Takenouti, Mechanism of anodic dissolution of iron-chromium alloys investigated by electrode impedances—I. Experimental results and reaction model, *Electrochim. Acta*, 31(1986), No. 9, p. 1147.

[11]   P. Marcus and J.M. Grimal, The anodic dissolution and pas-

sivation of NiCrFe alloys studied by ESCA, *Corros. Sci.*, 33(1992), No. 5, p. 805.

[12] C.S. Wang, C.Y. Tsai, C.G. Chao, and T.F. Liu, Effect of chromium content on corrosion behaviors of Fe–9Al–30Mn–(3,5,6.5,8)Cr–1C alloys, *Mater. Trans.*, 48(2007), No. 4, p. 2973.

[13] B. Jegdić, D.M. Dražić, and J.P. Popić, Open circuit potentials of metallic chromium and austenitic 304 stainless steel in aqueous sulphuric acid solution and the influence of chloride ions on them, *Corros. Sci.*, 50(2008), No. 5, p. 1235.

[14] K. Sugimoto and S. Matsuda, Passive and transpassive films on Fe–Cr alloys in acid and neutral solutions, *Mater. Sci. Eng.*, 42(1980), p. 181.

[15] I. Olefjord, The passive state of stainless steels, *Mater. Sci. Eng.*, 42(1980), p. 161.

[16] I. Olefjord, B. Brox, and U. Jelvestam, Surface composition of stainless steels during anodic dissolution and passivation studied by ESCA, *J. Electrochem. Soc.*, 132(1985), No. 12, p. 2854.

[17] J.A.L. Dobbelaar and J.H.W. de Wit, Impedance measurements and analysis of the corrosion of chromium, *J. Electrochem. Soc.*, 137(1990), No. 7, p. 2038.

[18] M. Metikoš-Huković and R. Babić, Passivation and corrosion behaviours of cobalt and cobalt-chromium-molybdenum alloy, *Corros. Sci.*, 49(2007), No. 9, p. 3570.

[19] M. Bojinov, G. Fabricius, T. Laitinen, T. Saario, and G. Sundholm, Conduction mechanism of the anodic film on chromium in acidic sulphate solutions, *Electrochim. Acta*, 44(1998), No. 2-3, p. 247.

[20] H.H. Uhlig, Fundamental factors in corrosion control, *Corrosion*, 4(1947), No. 3, p. 173.

[21] H.H. Uhlig, Passivity in metals and alloys, *Corros. Sci.*, 19(1979), No. 7, p. 777.

[22] V.M. Kolotyrkin, Electrochemical behaviour and anodic passivity mechanism of certain metals in electrolyte solutions, *Z. Elektrochem.*, 62(1958), No. 6-7, p. 664.

[23] R.D. Armstrong, M. Henderson, and H.R. Thirsk, The impedance of chromium in the active-passive transition, *J. Electroanal. Chem. Interfacial Electrochem.*, 35(1972), No. 1, p. 119.

[24] M.S. El-Basiouny and S. Haruyama, The polarization behaviour of chromium in acidic sulphate solutions, *Corros. Sci.*, 17(1977), No. 5, p. 405.

[25] M. Okuyama, M. Kawakami, and K. Ito, Anodic dissolution of chromium in acidic sulphate solutions, *Electrochim. Acta*, 30(1985), No. 6, p. 757.

[26] L. Björnkvist and I. Olefjord, The electrochemistry of chromium in acidic chloride solutions: Anodic dissolution and passivation, *Corros. Sci.*, 32(1991), No. 2, p. 231.

[27] M. Seo, R. Saito, and N. Sato, Ellipsometry and auger analysis of chromium surfaces passivated in acidic and neutral aqueous solutions, *J. Electrochem. Soc.*, 127(1980), No. 9, p. 1909.

[28] T.P. Moffat and R.M. Latanision, An electrochemical and X-Ray photoelectron spectroscopy study of the passive state of chromium, *J. Electrochem. Soc.*, 139(1992), No. 7, p. 1869.

[29] B. Stypula and J. Banaś, Passivity of chromium in sulphuric acid solutions, *Electrochim. Acta*, 38(1993), No. 15, p. 2309.

[30] V. Maurice, W.P. Yang, and P. Marcus, XPS and STM Investigation of the passive film formed on Cr(110) single-crystal surfaces, *J. Electrochem. Soc.*, 141(1994), No. 11, p. 3016.

[31] D. Zuili, V. Maurice, and P. Marcus, In situ scanning tunneling microscopy study of the structure of the hydroxylated anodic oxide film formed on Cr(110) single-crystal surfaces, *J. Phys. Chem. B*, 103(1999), No. 37, p. 7896.

[32] H. Ma, X.Q. Chen, R.H. Li, S.L. Wang, J.H. Dong, and W. Ke, First-principles modeling of anisotropic anodic dissolution of metals and alloys in corrosive environments, *Acta Mater.*, 130(2017), p. 137.

[33] N. Sato, An overview on the passivity of metals, *Corros. Sci.*, 31(1990), p. 1.

[34] J.L. Lv and T.X. Liang, The effect of passivated potential on the passive films formed on pure chromium in borate buffer solution, *Surf. Interface Anal.*, 49(2017), No. 6, p. 533.

[35] C.O. Olsson and D. Landolt, Passive films on stainless steels—chemistry, structure and growth, *Electrochim. Acta*, 48(2003), No. 9, p. 1093.

[36] J.A.L. Dobbelaar and J.H.W. de Wit, The corrosion behavior of polycrystalline and single crystal chromium a revised model, *J. Electrochem. Soc.*, 139(1992), No. 3, p. 716.

[37] D. Caplan and G.I. Sproule, Effect of oxide grain structure on the high-temperature oxidation of Cr, *Oxid. Met.*, 9(1975), No. 5, p. 459.

[38] M. Liu, D. Qiu, M.C. Zhao, G.L. Song, and A. Atrens, The effect of crystallographic orientation on the active corrosion of pure magnesium, *Scripta Mater.*, 58(2008), No. 5, p. 421.

[39] G.L. Song and Z.Q. Xu, Effect of microstructure evolution on corrosion of different crystal surfaces of AZ31 Mg alloy in a chloride containing solution, *Corros. Sci.*, 54(2012), p. 97.

[40] L.D. Chen, J.K. Nørskov, and A.C. Luntz, Al-Air batteries: Fundamental thermodynamic limitations from first-principles theory, *J. Phys. Chem. Lett.*, 6(2015), No. 1, p. 175.

[41] L.D. Chen, J.K. Nørskov, and A.C. Luntz, Theoretical limits to the anode potential in aqueous Mg–air batteries, *J. Phys. Chem. C*, 119(2015), No. 34, p. 19660.

[42] J.S. Hummelshoj, A.C. Luntz, and J.K. Nørskov, Theoretical evidence for low kinetic overpotentials in Li–O$_2$ electrochemistry, *J. Chem. Phys.*, 138(2013), art. No. 034703.

[43] V. Viswanathan, J.K. Norskov, A. Speidel, R. Scheffler, S. Gowda, and A.C. Luntz, Li–O$_2$ kinetic overpotentials: Tafel plots from experiment and first-principles theory, *J. Phys. Chem. Lett.*, 4(2013), No. 4, p. 556.

[44] J.K. Nørskov, J. Rossmeisl, A. Logadottir, L. Lindqvist, J.R. Kitchin, T. Bligaard, and H. Jónsson, Origin of the overpotential for oxygen reduction at a fuel-cell cathode, *J. Phys. Chem. B*, 108(2004), No. 46, p. 17886.

[45] J. Rossmeisl, J.K. Nørskov, C.D. Taylor, M.J. Janik, and M. Neurock, Calculated phase diagrams for the electrochemical oxidation and reduction of water over Pt(111), *J. Phys. Chem. B*, 110(2006), No. 43, p. 21833.

[46] S. Meng, E.G. Wang, and S.W. Gao, Water adsorption on metal surfaces: a general picture from density functional theory studies, *Phys. Rev. B*, 69(2004), art. No. 195404.

[47] A. Michaelides and K. Morgenstern, Ice nanoclusters at hydrophobic metal surfaces, *Nat. Mater.*, 6(2007), p. 597.

[48] G.S. Karlberg, J. Rossmeisl, and J.K. Nørskov, Estimations of electric field effects on the oxygen reduction reaction based on the density functional theory, *Phys. Chem. Chem. Phys.*, 9(2007), No. 37, p. 5158.

[49] P. Giannozzi, S. Baroni, N. Bonini, *et al.*, QUANTUM ESPRESSO: a modular and open-source software project for quantum simulations of materials, *J. Phys. Condens. Matter*, 21(2009), No. 39, art. No. 395502.

[50] S.R. Bahn and K.W. Jacobsen, An object-oriented scripting interface to a legacy electronic structure code, *Comput. Sci. Eng.*, 4(2002), No. 3, p. 56.

[51] D. Vanderbilt, Soft self-consistent pseudopotentials in a generalized eigenvalue formalism, *Phys. Rev. B*, 41(1990), p. 7892.

[52] B. Hammer, L.B. Hansen, and J.K. Nørskov, Improved adsorption energetics within density-functional theory using revised Perdew-Burke-Ernzerhof functionals, *Phys. Rev. B*, 59(1999), p. 7413.

[53] H.J. Monkhorst and J.D. Pack, Special points for Brillouin-zone integrations, *Phys. Rev. B*, 13(1976), p. 5188.

[54] S. Siahrostami, V. Tripkovic, K.T. Lundgaard, K.E. Jensen, H.A. Hansen, J.S. Hummelshøj, J.S.G. Mýrdal, T. Vegge, J.K. Nørskov, and J. Rossmeisl, First principles investigation of zinc-anode dissolution in zinc-air batteries, *Phys. Chem. Chem. Phys.*, 15(2013), No. 17, p. 6416.

[55] H.A. Hansen, J. Rossmeisl, and J.K. Nørskov, Surface pourbaix diagrams and oxygen reduction activity of Pt, Ag and Ni(111) surfaces studied by DFT, *Phys. Chem. Chem. Phys.*, 10(2008), p. 3722.

[56] S.G. Bratsch, Standard electrode potentials and temperature coefficients in water at 298.15 K, *J. Phys. Chem. Ref. Data*, 18(1989), p. 1.

[57] J.K. Nørskov, F. Studt, F. Abild-Pedersen, and T. Bligaard, Fundamental Concepts in Heterogeneous Catalysis, John Wiley & Sons, USA, 2014.